Fusion of ^{124,132}Sn with ^{40,48}Ca

J. J. Kolata, A. Roberts, A. M. Howard, D. Shapira, J. F. Liang, C. J. Gross, R. L. Varner, Z. Kohley, A. N. Villano, H. Amro, W. Loveland, and E. Chavez

Phys. Rev. C **85**, 054603 — Published 2 May 2012

DOI: 10.1103/PhysRevC.85.054603

Fusion of ^{124,132}Sn with ^{40,48}Ca

J. J. Kolata*, A. Roberts, and A.M. Howard

Physics Department, University of Notre Dame, Notre Dame, IN 46556-5670

D. Shapira, J.F. Liang, C.J. Gross, R.L. Varner, and Z. Kohley†

Physics Division, Oak Ridge National Laboratory, Oak Ridge, TN 37831

A.N. Villano‡ and H. Amro§

Physics Department, University of Michigan, Ann Arbor, MI 48109-1090

W. Loveland

Department of Chemistry, Oregon State University, Corvallis, OR 97331-4003

E. Chavez

IFUNAM, A.P. 20-364, México 01000

Abstract

Fusion excitation functions for the reactions of ^{124,132}Sn with ^{40,48}Ca were measured at energies near to and below the Coulomb barrier. Weak sub-barrier fusion enhancement accounted for by coupling to the first 2^+ and 3^- states in the target and projectile was observed for ^{124,132}Sn+^{48}Ca. However, the ^{124,132}Sn+^{40}Ca fusion cross sections are very strongly enhanced below the barrier and this difference survives even after correcting for trivial size effects. Although the enhancement appears to be related to the existence of large positive Q-values for neutron transfer reactions, it is not proportional to the magnitudes of those Q-values, which are much larger for ^{132}Sn+^{40}Ca than for ^{124}Sn+^{40}Ca.

PACS numbers: 25.60.-t, 25.60.Pj, 25.70.Jj

Keywords: exotic nucleus, fusion-evaporation

* jkolata@nd.edu

† Present address: NSCL, Michigan State University, East Lansing, MI 48824

‡ Present address: Physics Department, University of Minnesota, Minneapolis, MN 55455

§ Present address: Henry Ford Health Systems, Henry Ford Hospital, Detroit, MI 48202

I. INTRODUCTION

Large enhancements of the sub-barrier fusion yields have been observed in a number of systems that have positive Q-values for neutron transfer [1]-[6]. The goal in the present work was to compare the fusion of stable ^{124}Sn and radioactive ^{132}Sn on the same targets in order to study the effects of neutron excess and neutron-transfer Q-values on fusion. The Ca isotopes are ideal for this purpose since the ^{40}Ca+Sn systems have many positive neutron-transfer Q-values while all the corresponding channels for ^{48}Ca+Sn display negative Q-values. Furthermore, an identical ^{172}Yb composite system can be produced using two essentially spherical targets, thus reducing deformation effects on fusion. Data already exist for ^{40}Ca+^{124}Sn [2]. This reaction has many positive Q-value channels and the corresponding fusion cross sections are known to be strongly enhanced below the barrier. It is therefore of special interest to compare these data to the ^{40}Ca+^{132}Sn case, where the positive particle-transfer Q-values are even larger and more numerous as illustrated in Tables I-IV. (Note that these are Q-values for ground state to ground state transitions). Many of these channels were observed with significant strength in a study of ^{40}Ca+^{124}Sn multinucleon transfer reactions [7]. The definitions of "pickup" and "stripping" reactions are as given in that paper, *i.e*, in terms of transfer to or from the light partner in the reaction. Channels involving neutron stripping or proton pickup all have negative Q-values.

TABLE I: Q-values for neutron pickup channels (MeV).

	^{40}Ca+^{124}Sn	^{48}Ca+^{124}Sn	^{40}Ca+^{132}Sn	^{48}Ca+^{132}Sn
1n	-0.125	-3.34	+1.05	-2.16
2n	+5.41	-2.93	+7.28	-1.06
3n	+4.53	-7.38	+7.60	-4.31
4n	+9.49	-8.84	+13.4	-4.92
5n	+7.80	-14.5	+12.9	-9.37

TABLE II: Q-values for proton stripping channels (MeV).

	^{40}Ca+^{124}Sn	^{48}Ca+^{124}Sn	^{40}Ca+^{132}Sn	^{48}Ca+^{132}Sn
1p	-1.02	-8.50	+1.35	-6.13
2p	+1.7	-12.7	+5.87	-8.49
3p	-2.34	-25.1	+4.15	-18.6
4p	-2.56	-33.5	+5.69	-25.2
5p	-10.7	-50.7	0	-40.0

TABLE III: Q-values for neutron pickup + proton stripping channels (MeV).

	^{40}Ca+^{124}Sn	^{48}Ca+^{124}Sn	^{40}Ca+^{132}Sn	^{48}Ca+^{132}Sn
1n-1p	-1.93	-12.7	+1.81	-8.97
1n-2p	-0.82	-17.5	+4.79	-11.9
1n-3p	-5.37	-29.8	+2.47	-22.0
1n-4p	-7.87	-40.9	+1.91	-31.1
1n-5p	-16.9	-58.6	-4.81	-46.5
2n-1p	+1.7	-12.9	+6.15	-8.46
2n-2p	+2.48	-18.2	+8.82	-11.9
2n-3p	-4.45	-33.1	+4.29	-24.4
2n-4p	-7.05	-44.0	+3.58	-33.3
2n-5p	-17.8	-64.1	-4.82	-51.1

II. EXPERIMENTAL METHOD

The fusion measurements were carried out in inverse kinematics using targets of ^{40,48}Ca and beams of ^{124,132}Sn. Evaporation residues were detected using the CSSER (Compact System for Studies of Evaporation Residues) setup [8] at Oak Ridge National Laboratory (ORNL). Two microchannel-plate timing detectors (MCPs) placed before the target were used to monitor the incident beam and provide a timing reference. A third, position-sensitive

TABLE IV: Q-values for neutron pickup + proton stripping channels, continued (MeV).

	^{40}Ca+^{124}Sn	^{48}Ca+^{124}Sn	^{40}Ca+^{132}Sn	^{48}Ca+^{132}Sn
3n-1p	+0.27	-18.8	+5.91	-13.1
3n-2p	-0.84	-25.1	+6.88	-17.4
3n-3p	-8.16	-40.4	+1.86	-30.4
3n-4p	-12.7	-53.3	-0.59	-41.1
4n-1p	+3.10	-20.8	+9.82	-14.1
4n-2p	+1.65	-27.6	+10.4	-18.9
4n-3p	-7.83	-44.8	+3.35	-33.6
4n-4p	-12.6	-58.0	+0.75	-44.7
4n-5p	-26.1	-73.7	-10.4	-58.0

MCP after the target detected both the incident beam and the evaporation residues. The main trigger for the data-collection system was arranged so that only particles that were significantly slower than the beam (primarily the evaporation residues) were counted. However, fast-particle events (primarily the beam) were down-scaled by a factor of 1000 and generated a secondary trigger that was used to measure the incident beam intensity. Finally, the beam and reaction products entered a segmented ion chamber which provided energy-loss and total energy information that could be used to determine the Z of the ions. This system is discussed in detail in Ref. [8], which provides numerous examples of diagrams and plots illustrating its operation. The only significant difference from the setup described there was the fact that the distance from the target to the third timing detector was increased from 169 mm to 329 mm in order to provide a sufficient path length to cleanly separate the evaporation residues, which are faster than those in the Ni+Sn experiments. This slightly reduced the efficiency for detection of evaporation residues because of the smaller angular aperture of the ion chamber, but this was partially counteracted by the fact that the angular spread of the residues in the laboratory system (computed using the evaporation code PACE2 [9]) was smaller. The computed efficiencies (which also included the effect of multiple scattering in the targets) ranged from 86.9% to 99.7% depending on the incident beam energy and

target thickness, compared with 93% to 98% in the ^{132}Sn+^{64}Ni experiment [10].

The Sn beams were produced using the Holifield Radioactive Ion Beam Facility (HRIBF) at ORNL. The purity of the stable ^{124}Sn beam was 100% and its intensity was limited to <100,000 particles per second (pps) due to the rate limitation of the ion chamber. Studies were carried out to insure that CSSER could comfortably handle this rate. The radioactive ^{132}Sn beam had a purity of >95%, and its intensity ranged from 50,000 to 100,000 pps. (See Ref. [10] for a discussion of the method used to obtain and measure this high purity, which requires suppression of the ^{132}Te isobar).

The isotopic purity of the targets was 99.98% for ^{40}Ca and 97.16% for ^{48}Ca. Because of concerns about the stability of pure Ca targets, it was decided to use CaF_2 instead. A test experiment was carried out to make sure that Sn+F evaporation products could easily be separated from the products of interest. The ^{48}Ca was originally in metallic form, and it was converted to the fluoride at LNL-Legnaro in Italy where the targets were produced. The ^{40}Ca material was in the form of the carbonate ($CaCO_3$), which was first converted to the fluoride at ORNL. The nominal thicknesses of the targets were 251 and 628 μg/cm^2 for ^{40}Ca and 361 μg/cm^2 for ^{48}Ca as measured at LNL-Legnaro (assumed to be CaF_2), evaporated onto 15 μg/cm^2 C backings. However, it became clear during the course of the first ^{124}Sn+^{40}Ca experiment that the targets were actually much thicker and the stoichiometry was not CaF_2, as determined by energy-loss measurements using the Sn beams and a ^{241}Am α-particle source and by an inability to reproduce the existing ^{124}Sn+^{40}Ca data [2]. We first decided to repeat the measurement using a 240 μg/cm^2 target of natural CaF_2 evaporated onto a 20 μg/cm^2 C backing. The thickness of this target was initially determined using a ^{241}Am α-particle source. It is essential to know both the thickness and stoichiometry of the target due to the fact that the energy loss of Sn beams is large (*e.g.*, 28 MeV for a 500 μg/cm^2 $^{40}CaF_2$ target and a 500 MeV ^{132}Sn beam). The energy loss corrections were determined according to the iterative technique described in detail in Ref. [10]. Corrections for the energy loss in the C foils in the two upstream MCP detectors and the target backing were also applied. The results of this experiment were very encouraging; the data from Ref. [2] were well reproduced (see Fig. 1), especially considering the ±15% systematic error assigned to the fusion cross sections in that work. Our results suggest that this error may have been over-estimated.

Next, we analyzed the compositions of the targets via the Rutherford back-scattering

(RBS) technique using the 1.75 MV tandem accelerator at Hope College in Holland, MI. It was found that the thickness of the natural Ca target was consistent with that determined from the α-particle energy loss measurement, and that its stoichiometry was consistent with CaF_2. A thin flash of Au was found on the backing, but this did not significantly affect the results of the ^{124}Sn+^{nat}Ca experiment. The actual thickness of the ^{48}Ca target was found to be 461 μg/cm^2 and its stoichiometry was approximately consistent with CaF_2, but with small contaminants of C and O. The two ^{40}Ca targets, however, were not only much thicker than their nominal values but also displayed a higher degree of C and O contamination, perhaps coming from residual $CaCO_3$ remaining after conversion to the fluoride. The thicknesses of these two targets were found to be 466 and 974 μg/cm^2, compared with their nominal thicknesses of 251 and 628 μg/cm^2, respectively. The RBS thicknesses and compositions were used in the calculation of the energy losses and cross sections from all the targets. The systematic error in the absolute fusion cross sections due to the uncertainty in the Ca content of the targets is estimated to be 10%. The results for ^{124}Sn+^{40}Ca, after accounting for the actual target thicknesses, are shown in Fig. 1. They are consistent with the data from Ref. [2].

III. RESULTS

The fusion-evaporation excitation functions for ^{124}Sn+^{48}Ca, ^{132}Sn+^{40}Ca, and ^{132}Sn+^{48}Ca measured in this experiment are shown in Figs. 2, 3, and 4, respectively. The solid, black curves in Figs.1-4 are PACE2 [9] calculations of the absolute fusion-evaporation cross sections for the respective systems. The high-energy data for the ^{48}Ca target with both beams show the effect of the fission competition predicted by PACE2, which results in a flattening or reduction of the evaporation residue cross section. The low-energy data for all systems are well above the PACE2 predictions since this code does not allow for the possibility of fusion below the Coulomb barrier.

The green, dot-dashed curves in the figures are the result of Wong-model [11] fits to the experimental data. Since PACE2 predicts the onset of fission at E_{cm} $\approx$140 MeV for both beams with the ^{48}Ca target, we have only fitted the data up to this energy in these cases. The parameters, as well as the χ^2 per degree of freedom, deduced from the fits are given in Table V. The results imply that the Wong model is applicable to these data sets, and that

TABLE V: Wong-model fits to the experimental fusion excitation functions.

System	$\hbar\omega$ (MeV)	R (fm)	V_0 (MeV)	χ^2/d.f.
^{40}Ca+^{124}Sn	11.85±0.87	10.02±0.14	114.09±0.29	1.5
^{48}Ca+^{124}Sn	8.79±0.78	10.40±0.14	114.16±0.30	2.2
^{40}Ca+^{132}Sn	13.13±1.09	11.20±0.20	115.18±0.35	1.5
^{48}Ca+^{132}Sn	5.77±0.52	10.81±0.16	112.86±0.16	1.2

the quoted statistical errors are reasonably consistent with the observed spread in the data points. Note that the curvature of the barrier in this model ($\hbar\omega$) is very large for the ^{40}Ca target with both beams, indicating the large sub-barrier enhancement of the fusion cross section discussed below.

Before discussing other models, it's worthwhile to directly compare the data sets. In order to do this, the "trivial" size differences of the various systems must be factored out. We define a "reduced energy" equal to the center-of-momentum energy divided by the quantity $V_0 = Z_p Z_T/R$, where $R = A_p^{1/3}+A_T^{1/3}$. V_0 is proportional to the Coulomb barrier and the product $Z_p Z_T$=1000 for all the systems studied here. In addition, we define a "reduced cross section" equal to the fusion-evaporation cross section divided by R^2. Fig. 5 compares the reduced cross sections for ^{124,132}Sn beams incident on ^{40}Ca (upper panel) and ^{48}Ca (lower panel) targets. At first glance, the data sets appear to be quite similar, leading to the conclusion that there is little dependence on the neutron excess of the beam. However, there are subtle differences, discussed further below, that are related to the structure of the Sn isotopes. Note, for example, the differences in the curves on these plots, which are the Wong-model fits discussed above.

A more striking result emerges when we compare the ^{40,48}Ca data taken with the ^{124}Sn beam (lower panel) and the ^{132}Sn beam (upper panel) in Fig. 6. Clearly, the ^{40}Ca data display reduced cross sections that are dramatically different from those taken with the ^{48}Ca target, for both beams. This behavior is consistent with the idea that the sub-barrier fusion cross section will be enhanced for those systems that have many positive Q-value neutron transfer channels, which in this case are those involving the ^{40}Ca target. In contrast, all the neutron transfer channels for both systems involving ^{48}Ca have a negative Q-value. However,

the Q-values for ^{40}Ca+^{132}Sn are much more positive than those for ^{40}Ca+^{124}Sn, while the sub-barrier enhancement is rather similar in the two cases. Apparently, the magnitude of the enhancement is not very sensitive to either the neutron excess of the beam or to the magnitude of the positive Q-values for neutron transfer.

In discussing the effect of channel coupling on sub-barrier fusion, "barrier distributions" [12] deduced from experimental cross sections are quite helpful in achieving an understanding of the coupling process. This method is applied in Ref. [2] to their ^{40}Ca+^{124}Sn data. Unfortunately, it involves taking the second derivative of the experimental excitation function. This means that excellent statistics and small energy steps are required, and it is impossible to obtain the required precision with the current generation of radioactive beam facilities. An alternative is to apply the method to Wong-model fits to the data. Since this model assumes a single parabolic barrier, the kind of detail seen, *e.g.*, in the "barrier distribution" plots shown in Ref. [2] cannot be obtained. However, it is possible to deduce some information on the location and width of the effective barrier. Although the same information can in principle be obtained from the Wong-model parameters themselves, it is useful to be able to visualize the barrier profile. For example, the effective barriers for ^{124,132}Sn beams incident on ^{40}Ca (upper panel) and ^{48}Ca (lower panel) targets are shown in Fig. 7. The results from Ref. [2] are also shown for comparison purposes; the effective barrier deduced from our data agrees remarkably well with the barrier distribution given in that work. Note that "reduced" barriers are given in order to factor out the trivial size effect. The ^{40}Ca barriers are considerably broader than those for ^{48}Ca, which is the result of the sub-barrier enhancements seen in the ^{40}Ca+Sn excitation functions. The ^{48}Ca barriers are narrower, and the ^{48}Ca+^{132}Sn barrier is the narrowest of all. As discussed below, this is due to the fact that neither participant in this reaction has a strong, low-lying collective state. The ^{48}Ca+^{124}Sn barrier is somewhat broader due to the effect of coupling to the first 3^- state in ^{124}Sn which is collective. A different perspective on the effective barriers is illustrated in Fig. 8, which compares the ^{40,48}Ca+^{124}Sn (lower panel) and ^{40,48}Ca+^{132}Sn (upper panel) systems. It can be seen that the ^{40}Ca barrier is shifted to a lower reduced energy relative to ^{48}Ca in the case of the ^{124}Sn beam, presumably due to the coupling to the neutron transfer channels. A similar shift does not occur for the ^{132}Sn beam, though the ^{40}Ca barrier is broader in this case. Perhaps this is a clue that the reaction dynamics are different for these two systems.

TABLE VI: Optical-model potential used in the Fresco calculations.

V (MeV)	r_0 (fm)	a_0 (fm)	W (MeV)	r_I (fm)	a_I (fm)	r_c(fm)
166.	1.15	0.57	2.12	0.95	0.39	1.4

Since coupling to inelastic states in the target and/or projectile can cause an enhancement of the sub-barrier fusion cross section, coupled-channels Born approximation (CCBA) calculations of inelastic excitation were carried out by Scarlassara, *et al.* [2], who showed that the magnitude of this effect was far too small to account for the observed enhancement. We have carried out similar calculations for the systems studied in the present experiment using the code Fresco [13]. The optical-model parameters for these calculations were obtained by fitting the fusion cross sections for ^{40}Ca+^{124}Sn predicted by PACE2 in the energy region well above the barrier, which are consistent with the experimental data for this system (see Fig. 1). The results are shown in Table VI. The reduced radii (r_0,r_I,r_c) were multiplied by $A_p^{1/3}$+$A_T^{1/3}$. The Coulomb potential was calculated for the usual charged sphere, and both the real and imaginary potentials were of the Woods-Saxon form. This parameter set was used in all the calculations reported here.

The Coulomb matrix elements M[Eλ] entered into Fresco, as well as the corresponding B[E$\lambda, \Uparrow$] in Weisskopf units (W.u.) (which provide a reference for the collectivity of the corresponding ground-state transitions), are listed in Table VII. They were taken from Refs. [14] (E2) and [15] (E3), except for the 2^+ and 3^- states in ^{132}Sn. The data for the 2^+ state in ^{132}Sn came from Ref. [16]. The M[E3] values for the 3^- states in ^{124}Sn and ^{132}Sn were assumed to be identical. Only an upper limit is known for the lifetime of the latter state, and the assumed matrix element is consistent with that limit. Only single-phonon transitions were included. Scarlassara, *et al.* [2] have shown that multiple excitations can be neglected in the calculation of the cross sections, though they do produce subtle effects on the barrier distributions. As noted above, we are not able to generate detailed barrier distributions from the current data sets. Coupling to the lowest 2^+ and 3^- states in both the projectile and the target were included. The corresponding nuclear deformation lengths δ_λ are also shown in Table VII. They were computed under the assumption that the Coulomb and nuclear deformation lengths are identical. The effect of the coupling on the fusion cross

TABLE VII: Parameters used in the Fresco calculations.

Isotope	State	E_x(MeV)	λ	B[E$\lambda, \Uparrow$](W.u.)	M[Eλ](e fm$^\lambda$)	δ_λ(fm)
^{40}Ca	2^+	3.90	2	2.36	9.80	0.52
^{40}Ca	3^-	3.74	3	30.65	142.8	1.94
^{48}Ca	2^+	3.83	2	1.62	9.17	0.46
^{48}Ca	3^-	4.51	3	8.66	91.1	1.10
^{124}Sn	2^+	1.13	2	9.04	40.7	0.60
^{124}Sn	3^-	2.60	3	11.4	270.	0.69
^{132}Sn	2^+	4.04	2	5.51	33.2	0.48
^{132}Sn	3^-	4.35	3	10.1	270.	0.66

section is largely determined by the nuclear deformation length. Both the real and the imaginary parts of the optical-model potential were deformed.

The results of the CCBA calculations are shown in Figs. 1-4. In each case, the dotted, blue curves show the fusion cross sections predicted using the "bare" potential, while the red, dashed curves show the effect of the coupling. Substantial sub-barrier enhancement occurs for ^{40}Ca+^{124,132}Sn, though it is nowhere near the amount necessary to reproduce the experimental data. This effect is mainly due to coupling to the collective 3^- state in ^{40}Ca. The other two systems show much less inelastic enhancement due to the lack of low-lying collective states. We have not attempted to include the effect of multinucleon transfer in these calculations. An approximate calculation of the effect of these channels was given for ^{40}Ca+^{124}Sn in Ref. [2], but it is not feasible to carry out such a calculation with Fresco.

The fusion cross sections for ^{48}Ca+^{124}Sn and ^{40}Ca+^{132}Sn are compared in Fig. 9 as a function of the excitation energy in the compound nucleus ^{172}Yb. There is no indication that the properties of the compound nucleus play any role in the sub-barrier enhancement observed in the ^{40}Ca+^{132}Sn system. The two reactions populate vastly different regions of the compound nucleus, at quite high excitation energy. As a result, the below barrier excitation function for ^{40}Ca+^{132}Sn (enhanced) can't be explained by some property of the compound nucleus since the ^{48}Ca+^{124}Sn reaction (not enhanced) populates the same region of excitation energy but well above its barrier. In addition, the ^{40}Ca+^{124}Sn fusion reaction

populates a different compound nucleus, ^{164}Yb, but still shows an excitation function similar to that for ^{40}Ca+^{132}Sn.

Time-dependent Hartree-Fock (TDHF) calculations with no adjustable parameters have been performed for fusion of the ^{40}Ca+^{124}Sn and ^{48}Ca+^{132}Sn systems by Oberacker, *et al.* [17]. The results are shown in Figs. 1 and 4, respectively. In the former case, the predicted cross sections are approximately 25% higher than the experimental data. A second calculation was carried out to remedy a problem associated with the fact that TDHF predicts a deformed ground state for ^{124}Sn due to a lack of pairing. This calculation (TDHF+BCS) reduced the predicted cross section near the barrier but did not correct the over-prediction at higher energies. The prediction for ^{48}Ca+^{132}Sn (Fig. 4) is a "density-constrained" TDHF (DC-TDHF) calculation in which the TDHF results above the barrier are used to deduce a nuclear potential that can then be used to compute sub-barrier fusion. The calculated cross sections above the barrier are higher than the experimental data, but by less than 10%. There is a bigger discrepancy in the region of the barrier where peripheral reactions are expected to play an important role. This is very similar to the situation for ^{64}Ni+^{132}Sn that Umar and Oberacker have also studied [18]. In both cases, TDHF over-predicts the experimental cross section near the barrier but displays much better agreement both above and below it.

IV. SUMMARY

Fusion-evaporation cross sections have been measured in inverse kinematics for the ^{40,48}Ca+^{124,132}Sn systems in the region of the Coulomb barrier. The ^{40}Ca+^{124}Sn data were found to agree with previous measurements taken with a ^{124}Sn target [2]. Strong enhancement of the sub-barrier cross sections was observed for both systems involving a ^{40}Ca target. In contrast, ^{48}Ca+^{124,132}Sn both display relatively little enhancement when compared with, *e.g.*, CCBA calculations including inelastic excitation. This difference survives even when the respective excitation functions are corrected for trivial size effects. On the other hand, the ^{40}Ca+^{124,132}Sn "reduced" cross sections appear to be similar throughout the range of this experiment, despite the fact that the magnitudes of the positive Q-values for neutron transfer are much larger for the ^{132}Sn beam. The reduced cross sections for ^{48}Ca+^{124,132}Sn are also similar to each other, but with a somewhat bigger discrepancy below the barrier.

The fusion cross sections for all four systems are well-fitted by the Wong model. The barrier parameters extracted from these fits display very large curvature $\hbar\omega$ for ^{40}Ca+^{124,132}Sn, indicative of large sub-barrier enhancements. The curvatures for ^{48}Ca+^{124,132}Sn are much smaller due to the lack of low-lying collective states in these cases. The positions and widths of the barriers were computed using the method described in Ref. [12], but applied to the Wong-model fits rather than the data themselves. This implies that only the general characteristics of the barriers, and not detailed "barrier distributions", could be extracted. When corrected for trivial size effects, the barrier for ^{40}Ca+^{124}Sn was observed to be shifted to lower energy relative to that for ^{48}Ca+^{124}Sn. However, a similar shift was not apparent for the ^{132}Sn beam.

Coupled-channels calculations for inelastic excitation of the first 2^+ and 3^- states in both the target and projectile have been carried out. The results show that the sub-barrier cross sections are enhanced by coupling to the inelastic excitations, but by not nearly enough to account for the ^{40}Ca+^{124,132}Sn data in agreement with the conclusions of Ref. [2]. The main cause of this enhancement was coupling to the collective 3^- state in ^{40}Ca. The other two systems show relatively little inelastic-coupling enhancement due to the lack of low-lying collective states.

States at high excitation energy in ^{172}Yb are populated by both ^{48}Ca+^{124}Sn and ^{40}Ca+^{132}Sn. Comparison of the associated fusion cross sections as a function of excitation energy demonstrates that properties of the compound nucleus do not play a role in the observed sub-barrier fusion enhancement for the latter system. The data have also been compared with the TDHF calculations of Oberacker, *et al.*[17]. It was found that the comparison between theory and experiment for ^{48}Ca+^{132}Sn is very similar to that obtained for ^{64}Ni+^{132}Sn in calculations by the same group [18]. In both these cases, there is good agreement both above and below the barrier, but the theory over-predicts the data in the immediate vicinity of the barrier. One major difference between these two systems is that the fission barrier is much closer to the Coulomb barrier for the ^{64}Ni target so the sum of fusion+fission was compared with the theory in that case.

In a recent Letter, Kohley, *et al.* [19] have shown that the near- and sub-barrier fusion yields for several Ni+Sn and Te+Sn systems are all very similar when displayed as reduced cross sections, despite the fact that there are many positive Q-value neutron channels for some of these systems while others have none. This is very different from the situation for

^{40}Ca+^{124,132}Sn in the present work, and for other systems in the literature [1]-[6], which show large sub-barrier enhancements when there are positive Q-value neutron transfer channels. In all these cases, which have a product of the nuclear charges $Z_pZ_T \leq 1000$, the enhancements survive even after correcting for size effects. Kohley, *et al.* [19] suggest the possibility that the increasing importance of deep-inelastic and quasi-fission reactions may be playing a role in the Ni+Sn and Te+Sn cases. This implies that the fusion of systems with charge product intermediate between Ca+Sn and Ni+Sn should be investigated.

Acknowledgments

This work has been partially supported by the US NSF under Grant No. PHY09-69456, and by the DOE Office of Nuclear Physics. The authors are indebted to Dr. Lorenzo Corradi and Massimo Loriggiola of LNL-Legnaro for producing the targets. We would also like to thank Drs. Paul DeYoung and Graham Peaslee of Hope College for helping us to carry out the RBS measurements. Finally, we would like to thank the HRIBF staff, and especially Dan Stracener, for providing the radioactive beam that was essential for this experiment.

---

[1] A.M. Stefanini, D. Ackermann, L. Corradi, J.N. He, G. Montagnoli, S. Beghini, F. Scarlassara, and G.F. Segato, Phys. Rev. C **52**, R1727 (1995).

[2] F. Scarlassara, S. Beghini, G. Montagnoli, G.F. Segato, D. Ackermann, L. Corradi, C.J. Lin, A.M. Stefanini, and L.F. Zheng, Nucl. Phys. **A672**, 99 (2000).

[3] M. Trotta, A.M. Stefanini, L. Corradi, A. Gadea, F. Scarlassara, S. Beghini, and G. Montagnoli, Phys. Rev. C **65**, 011601(R), (2001).

[4] A.M. Stefanini, B.R. Behara, S. Beghini, L. Corradi, E. Fioretto, A, Gadea, G. Montagnoli, N. Rowley, F. Scarlassara, S. Szilner, and M. Trotta, Phys. Rev. C **76**, 014610 (2007).

[5] Sunil Kalkal, S. Mandal, N. Madhavan, E. Prasad, Shashi Verma, A. Jhingan, Rohit Sandal, S. Nath, J. Gehlot, B. R. Behera, *et al.*, Phys. Rev. C **81**, 044610 (2010).

[6] H. Q. Zhang, C. J. Lin, F. Yang, H. M. Jia, X. X. Xu, Z. D. Wu, F. Jia, S. T. Zhang, Z. H. Liu, A. Richard, and C. Beck, Phys. Rev. C **82**, 054609 (2010).

[7] L. Corradi, J.H. He, D. Ackermann, A.M. Stefanini, A. Pisent, S. Beghini, G. Montagnoli,

F. Scarlassara, G.F. Segato, G. Pollarolo, G. Dasso, and A. Winther, Phys. Rev. C **54**, 201 (1996).

[8] D. Shapira, J.F. Liang, C.J. Gross, R.L. Varner, H. Amro, C. Harlin, J.J. Kolata, and S. Novotny, Nucl. Inst. and Methods in Physics Research **A551**, 330 (2005).

[9] A. Gavron, Phys. Rev C **21**, 230 (1980).

[10] J. F. Liang, D. Shapira, J. R. Beene, C. J. Gross, R. L. Varner, A. Galindo-Uribarri, J. Gomez del Campo, P. A. Hausladen, P. E. Mueller, D. W. Stracener, *et al.*, Phys. Rev. C **75**, 054607 (2007).

[11] C. Y. Wong, Phys. Rev. Lett. **31**, 766 (1973).

[12] N. Rowley, G.R. Satchler, and P.H. Stelson, Phys. Lett. **B254**, 25 (1991).

[13] I.J. Thompson, Comp. Phys. Rep. **7**, 167 (1988).

[14] S. Raman, C.H. Malarkey, W.T. Milner, C.W. Nestor, Jr., and P.H. Stelson, At. Data Nucl. Data Tables **36**,1 (1987).

[15] P.H. Spear, At. Data Nucl. Data Tables **42**, 55 (1989).

[16] R. L. Varner, J. R. Beene, C. Baktash, A. Galindo-Uribarri, C. J. Gross, J. Gomez del Campo, M. L. Halbert, P. A. Hausladen, Y. Larochelle and J. F. Liang, *et al.*, Eur. Phys. J. **A25**, Suppl. 1, 394 (2005).

[17] V.E. Oberacker, A.S. Umar, J.A. Maruhn, and P.-G. Reinhard, Phys. Rev. C **85**, 034609 (2012).

[18] A.S. Umar and V.E. Oberacker, Phys. Rev. C **76**, 014614 (2007).

[19] Z. Kohley, J. F. Liang, D. Shapira, R. L. Varner, C. J. Gross, J. M. Allmond, A. L. Caraley, E. A. Coello, F. Favela, K. Lagergren, and P. E. Mueller, Phys. Rev. Lett. **107**, 202701 (2011).

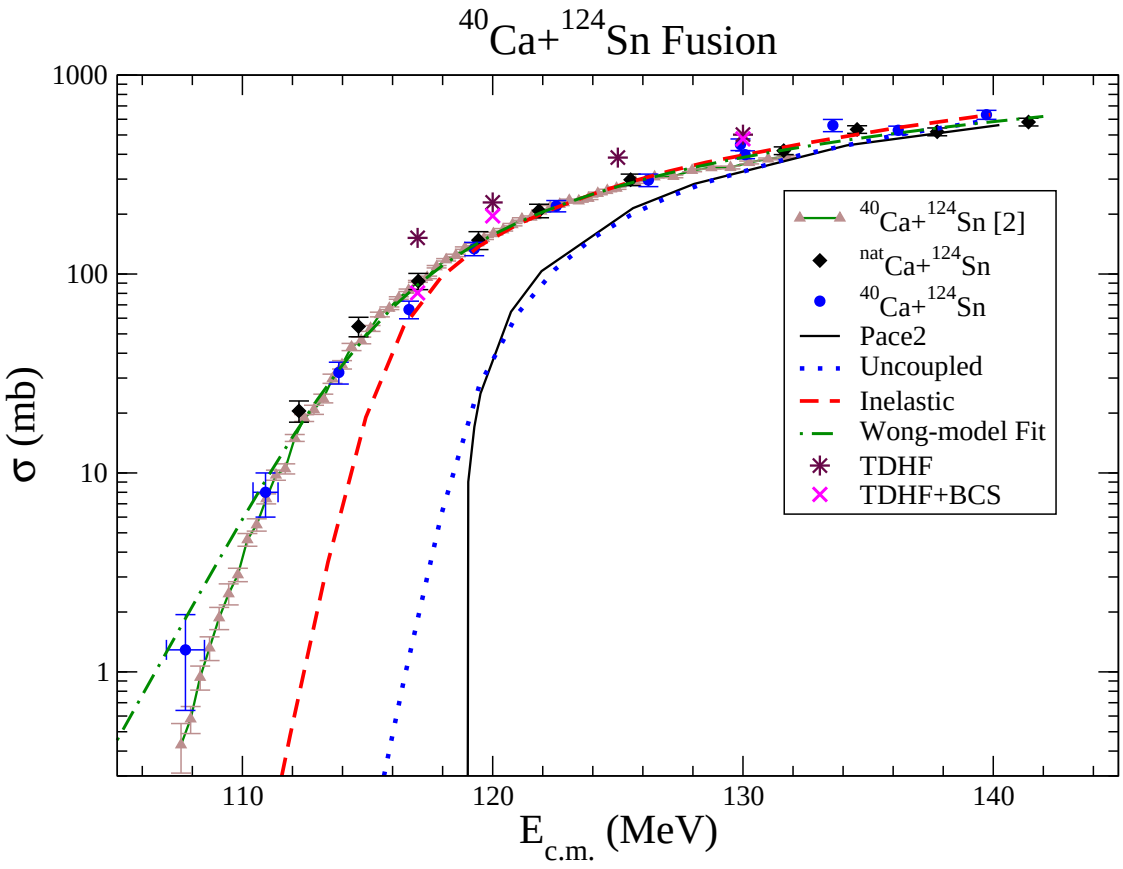

FIG. 1: (Color online) Fusion excitation functions for ^{124}Sn+^{40}Ca obtained with $^{40}CaF_2$ and $^{nat}CaF_2$ targets, compared with results from Ref. [2]. The various curves are discussed in the text.

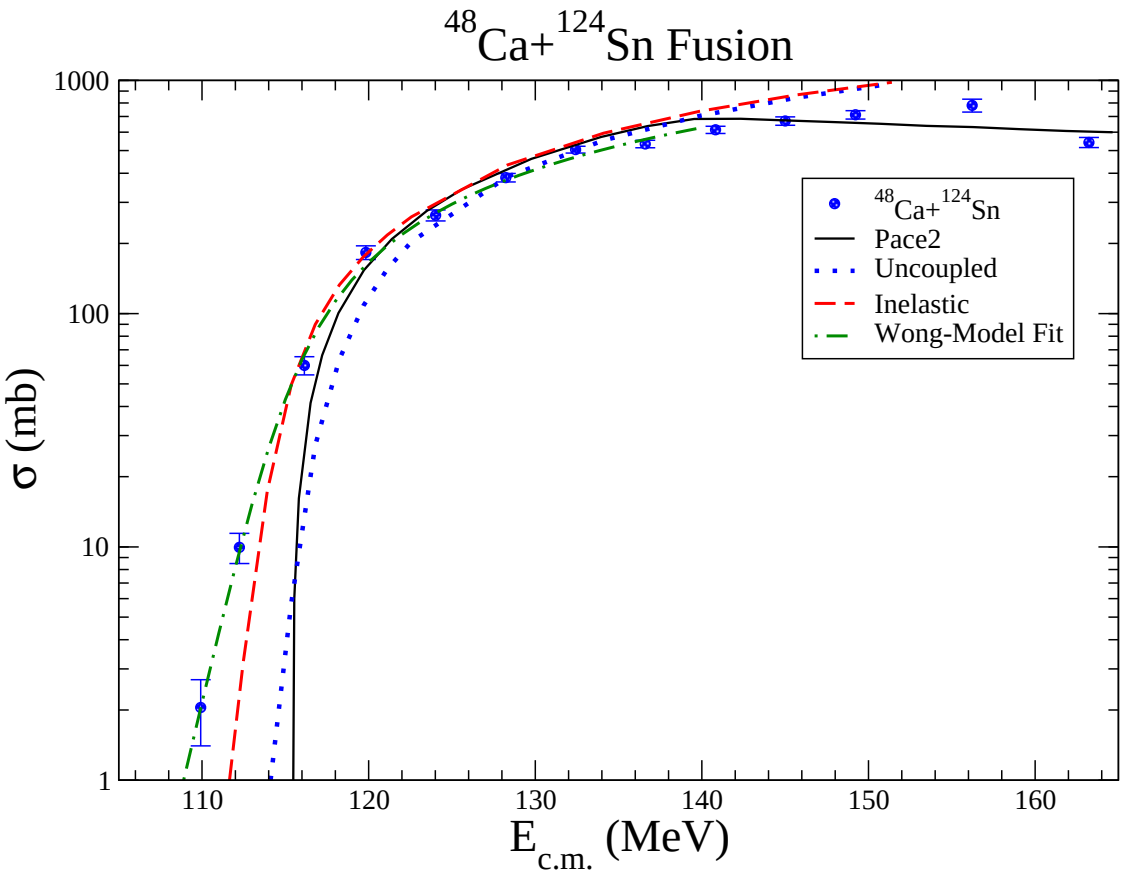

FIG. 2: (Color online) Fusion excitation functions for ^{124}Sn+^{48}Ca. The various curves are discussed in the text.

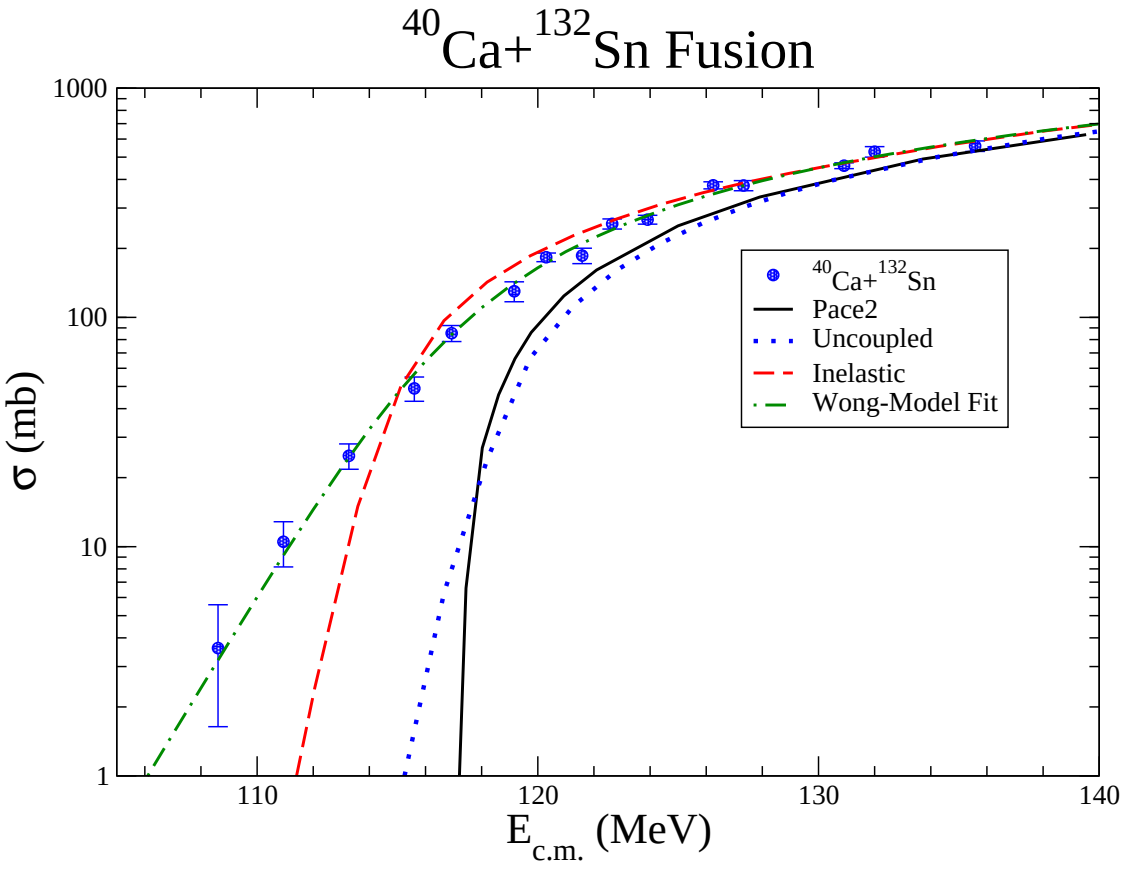

FIG. 3: (Color online) Fusion excitation functions for ^{132}Sn+^{40}Ca. The various curves are discussed in the text.

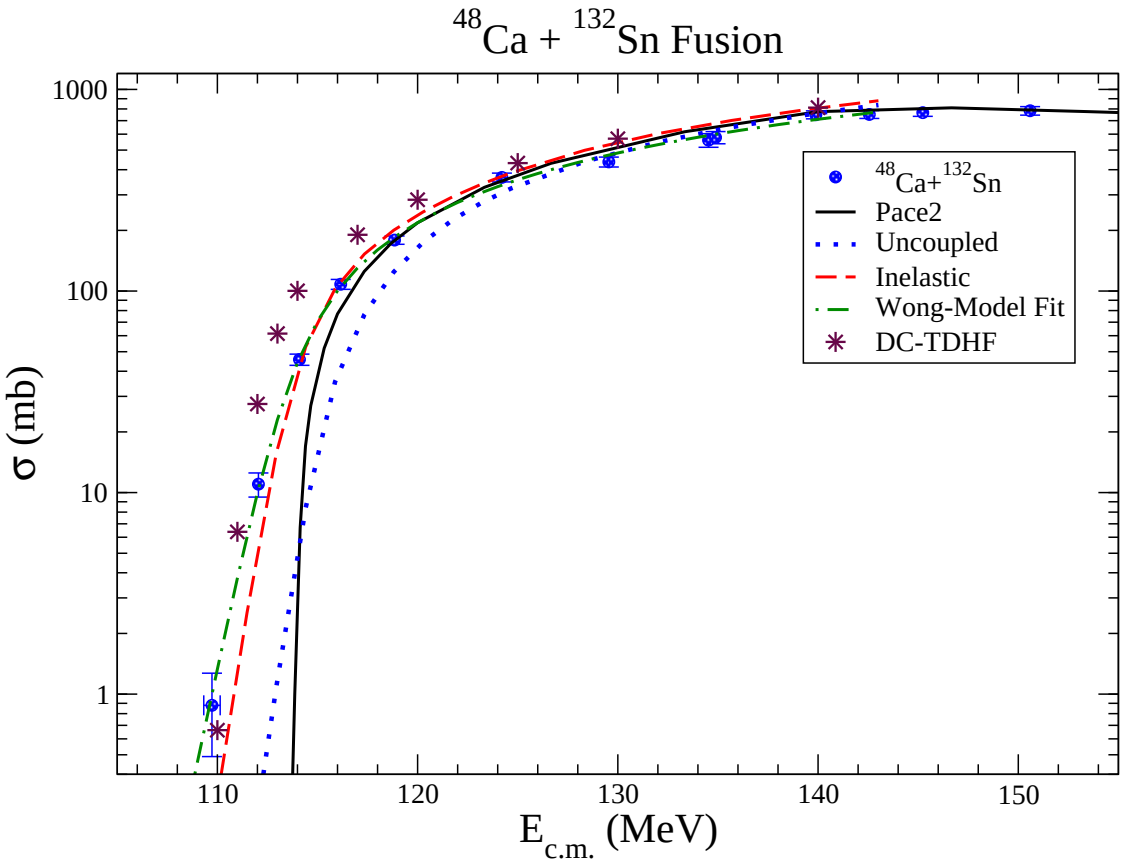

FIG. 4: (Color online) Fusion excitation functions for ^{132}Sn+^{48}Ca. The various curves are discussed in the text.

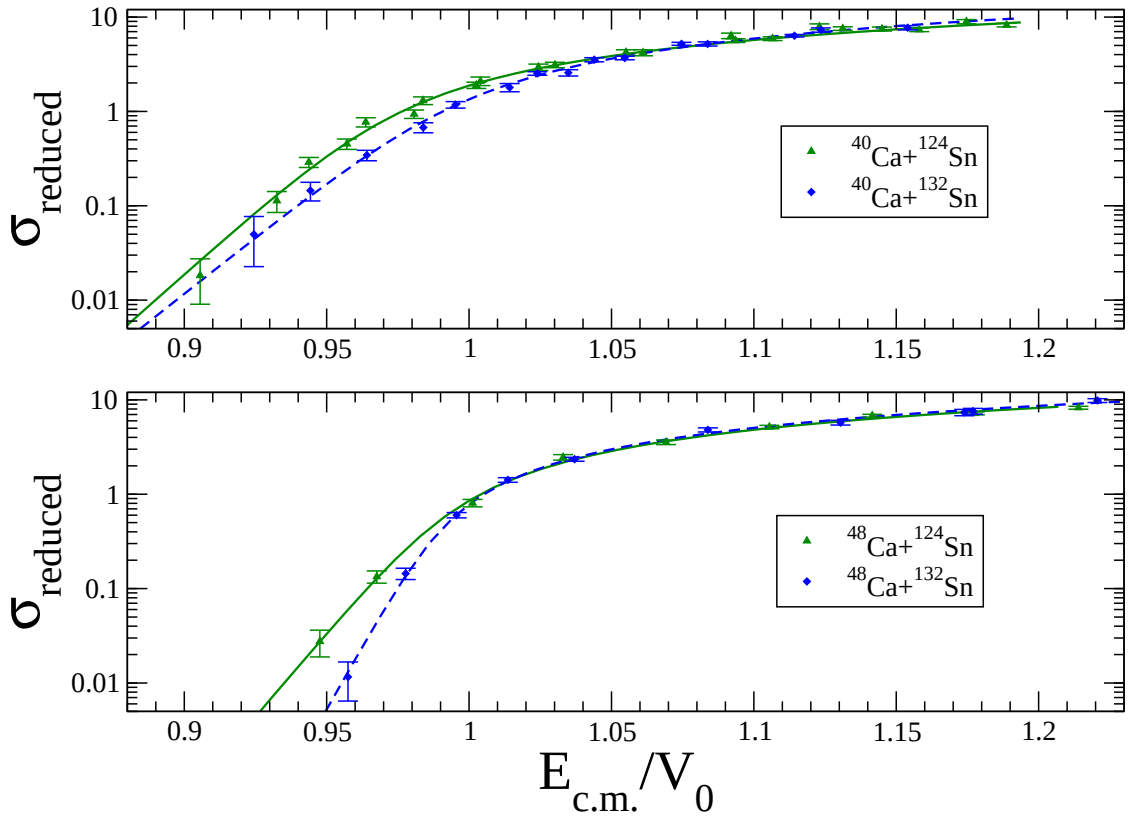

FIG. 5: (Color online) Reduced fusion excitation functions. The curves are the corresponding Wong-model fits.

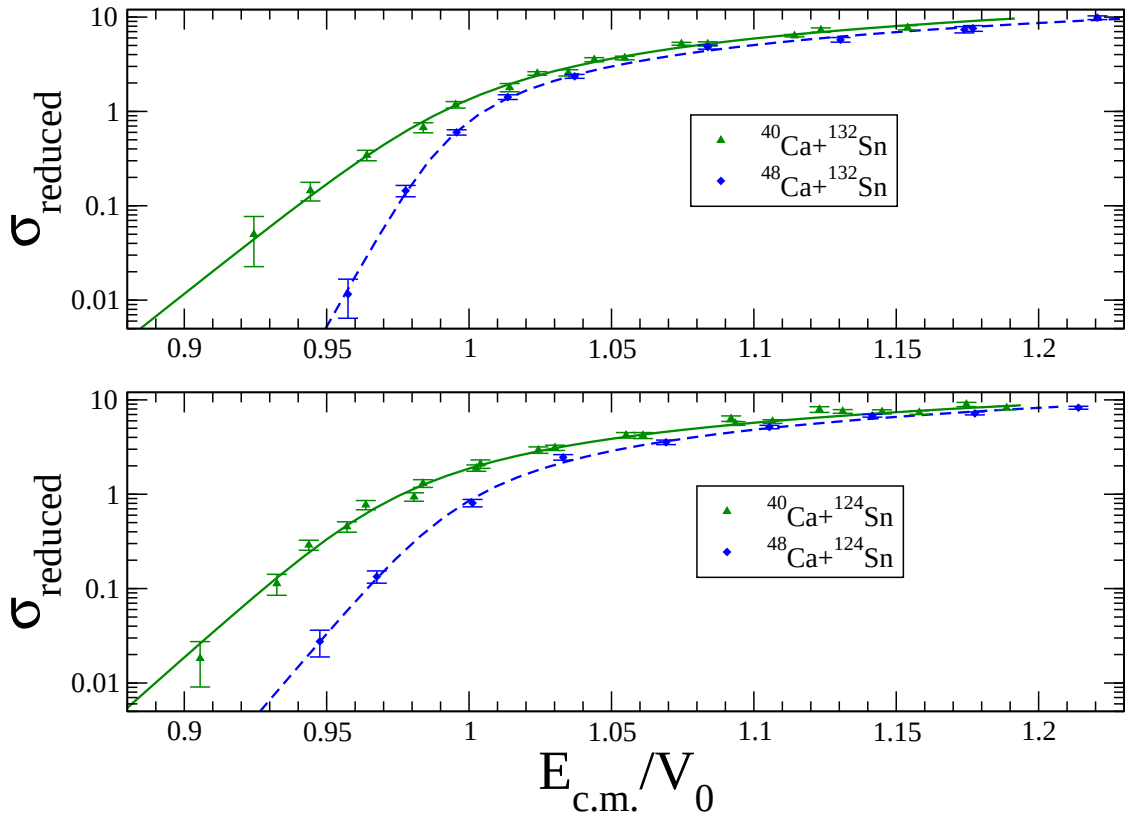

FIG. 6: (Color online) Reduced fusion excitation functions. The curves are the corresponding Wong-model fits.

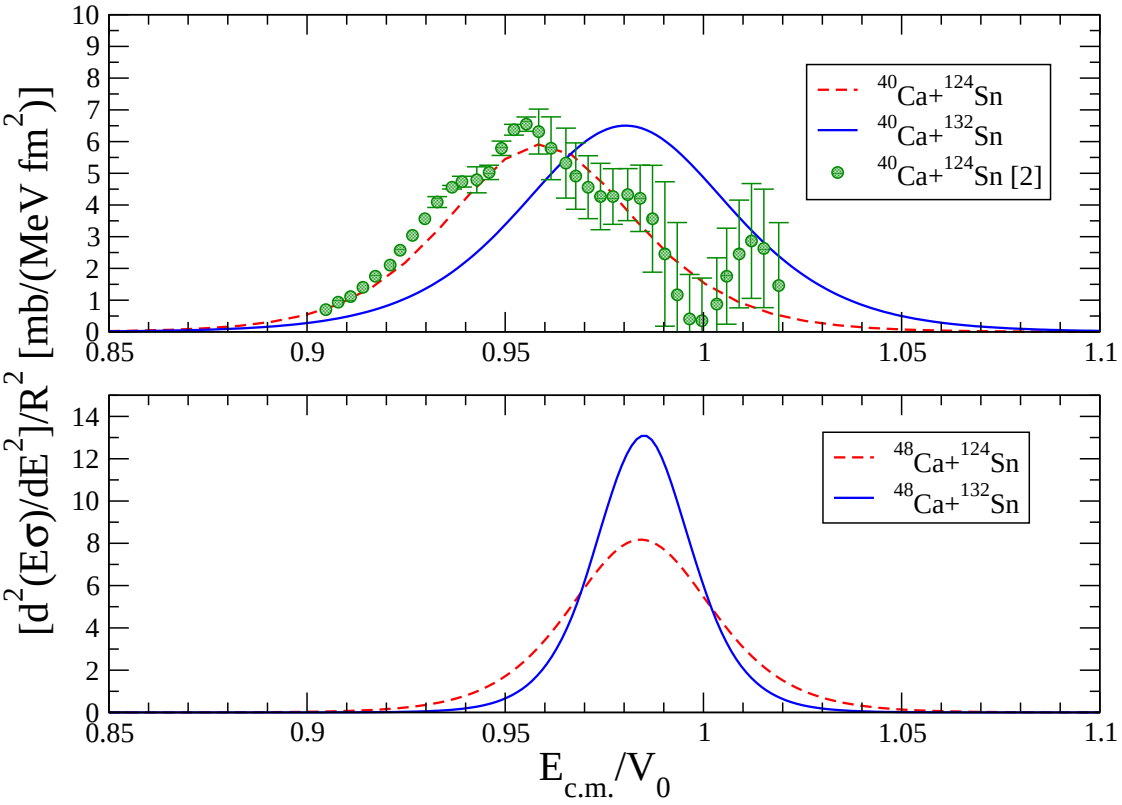

FIG. 7: (Color online) Barriers for Ca isotopes deduced from the Wong-model fits. The barrier profile for ^{40}Ca +^{124}Sn is compared with the barrier distribution data from Ref. [2].

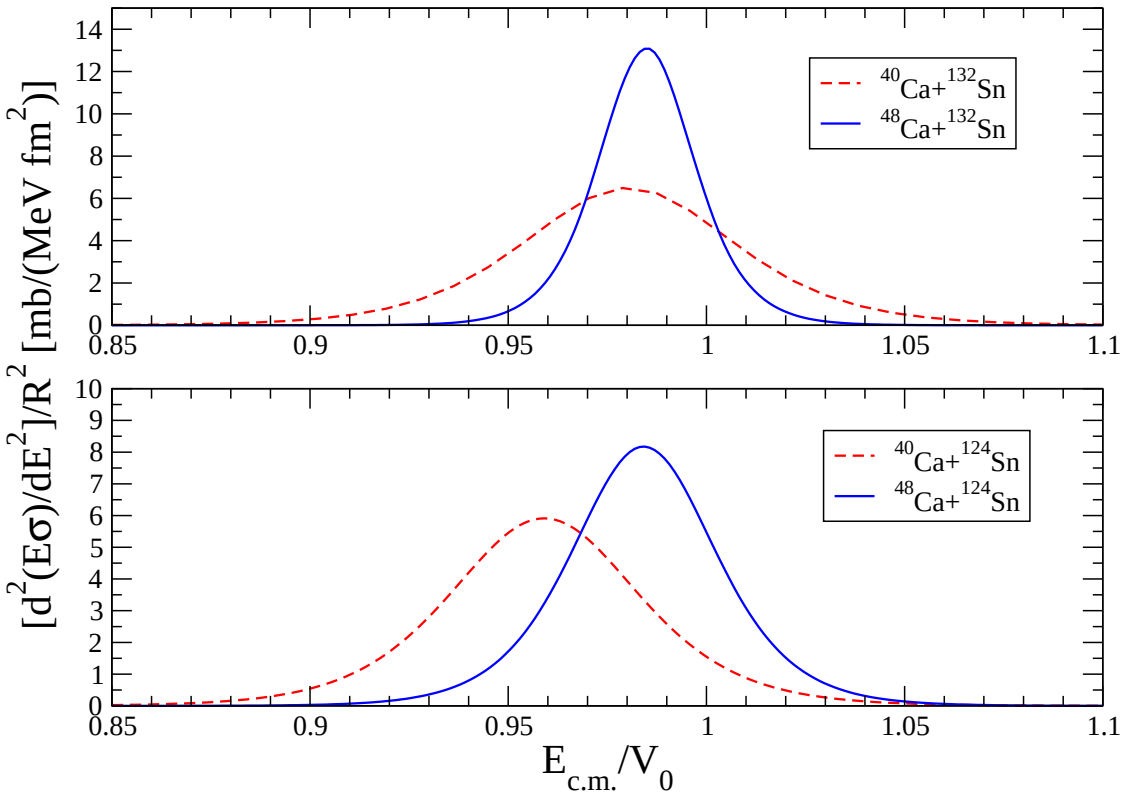

FIG. 8: (Color online) Barriers for Sn isotopes deduced from the Wong-model fits.

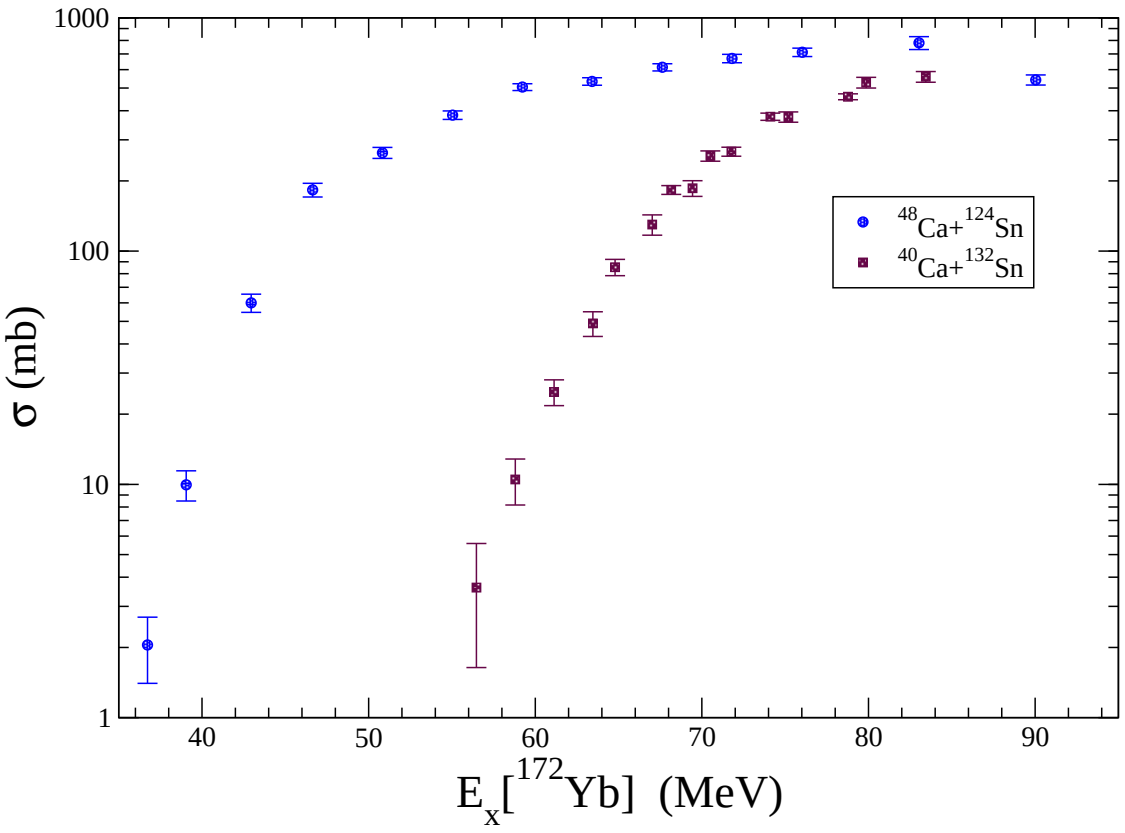

FIG. 9: (Color online) Fusion cross sections as a function of excitation energy in the compound nucleus.